Propagation effects of seeded collective emission by two-photon excited oxygen atoms

Xin Wang,[1,2] Yu-Hung Kuan,[3] Jun Jie Cui,[1] Yu Kun Yang,[4] Fan Xing,[2] Wen-Te Liao,[3,5,6] Luqi Yuan,[7] Yongjun Cheng,[1] Zeyang Liao,[2] Zheng Li,[8,9,10,*] and Song Bin Zhang[1,†]

[1]*School of Physics and Information Technology, Shaanxi Normal University, Xi'an 710119, China*
[2]*School of Physics, Sun Yat-Sen University, Guangzhou 510275, China*
[3]*Department of Physics, National Central University, Taoyuan City 32001, Taiwan, Republic of China*
[4]*School of Physics, Henan Normal University, Xinxiang 453007, China*
[5]*Physics Division, National Center for Theoretical Sciences, Taipei 10617, Taiwan, Republic of China*
[6]*Quantum Technology Center, National Central University, Taoyuan City 32001, Taiwan, Republic of China*
[7]*State Key Laboratory of Advanced Optical Communication Systems and Networks, School of Physics and Astronomy, Shanghai Jiao Tong University, Shanghai 200240, China*
[8]*State Key Laboratory for Mesoscopic Physics and Collaborative Innovation Center of Quantum Matter, School of Physics, Peking University, Beijing 100871, China*
[9]*Collaborative Innovation Center of Extreme Optics, Shanxi University, Taiyuan, Shanxi 030006, China*
[10]*Peking University Yangtze Delta Institute of Optoelectronics, Nantong, Jiangsu 226010, China*

(Received 4 July 2023; accepted 29 November 2023; published 26 December 2023)

A strong ultraviolet pumping laser propagating through the atmosphere could activate the medium and produce the forward and backward coherent air lasing. In this work, we present the theoretical analyses of forward and backward lasing dynamics in the long gain medium consisting of oxygen atoms. By numerically solving the semiclassical Maxwell-Bloch equations, we demonstrate that the atom density, the gain medium length, and the collisional decoherence rate substantially regulate the forward and backward air laser radiation at 845 nm. Especially, our study points out that lower atom density and moderate collisional decoherence rate are favorable for the backward radiation amplification in a long medium, since such conditions balance the competing processes of forward and backward radiation fields. The simulation shows that long medium backward air lasing becomes challenging in the oxygen atom system via double-photon pump, because the amplification can only occur around $z = 0$, and the amplified backward radiation does not carry the spectral information of atoms throughout the medium. On the other hand, certain mechanisms such as variation of backward-seeding delay could possibly alleviate the suppression of backward amplification.

DOI: 10.1103/PhysRevResearch.5.043293

I. INTRODUCTION

The collective laserlike emission can be formed when strong femtosecond laser pulses propagate in atomic or molecular gas. A prominent example is air lasing [1], which refers to a directed, pulsed laser radiation produced by remote pumping components in the air by a strong laser. It has the advantages of high brightness, good orientation, no restriction of resonator, and radiation occurs in both forward and backward direction [2,3]. Backward air lasing has important potential applications in atmospheric remote sensing, space detection, and environmental monitoring, particularly in geometries requiring single-ended standoff detection [4–7]. One of the fundamental mechanisms of air lasing is superfluorescence (SF) [8–13], which is a cooperative spontaneous radiation generated by large number of population-inverted atoms. Dicke first theoretically predicted the superradiation effect with high peak power [8].

Backward-propagating coherent superfluorescence can be generated by focusing forward-propagating laser beams in air [2,13–16]. A. Dogariu *et al*., who used 226 nm picosecond laser to dissociate the oxygen molecules in air into atoms and pump the dissociated oxygen atom to the excited state $3p\ ^3\mathrm{P}$, first reported the detection of 845 nm forward and backward air lasing in oxygen atoms on the order of millimeter propagation length in 2011 [2]. In the following year another experimental team achieved a laserlike emission source by pumping air with nanosecond pulses, producing 845 nm forward and backward superradiation pulses along a 1 cm cylindrical medium, which is proved to be a nonadiabatic atomic coherence process [14]. Yuan *et al*. theoretically simulated the forward and backward radiation process generated by picosecond and nanosecond pulse pumping oxygen atoms, and showed that the coherent radiation phenomena of atomic systems must be described by Maxwell-Bloch equations rather than rate equations [17]. It is proposed that the pulsed radiation can be attributed to the strongly oscillatory

*zheng.li@pku.edu.cn
†song-bin.zhang@snnu.edu.cn

superfluorescence produced by the coherent interaction between atoms [18–21].

In addition, by adding a light source in the forward and backward directions simultaneously, using a four-wave mixing mechanism, such as anti-Stokes Raman scattering to produce a backpropagation-coherent signal, the backward radiation of oxygen atoms can also be achieved [4,22]. Although this method is relatively simple, it requires a backward light source from the atmosphere, which limits its practical application. From the perspective of experiment and classical theory prediction, Liu *et al.* proposes that forward and backward radiation amplification of nitrogen molecular ion [23], and qualitatively explained the mechanism for the large backward radiation amplification under the pressure of 20 Mbar. Because of the backward and forward temporal asymmetry caused by the one-way propagation of the pump light through the excited medium, the backward radiation amplification only happened at lower gas pressure (about 10 Mbar). Furthermore, other methods are proposed for the implementation of backward air lasing [24,25], such as swept-gain excitation [26], which realizes the amplified backward signal by sending a series of pump pulses at different times. The pump pulse activates the gain medium via simultaneous population inversion, which is a consequence of the group velocity difference of pump light caused by medium scattering. Ding *et al.* also proved that the backward lasing signal in a flame can be significantly enhanced by 50% with plasma-forcing technique [27]. Moreover, it has been recently demonstrated that the forward air lasing process can be effectively modified by various quantum control schemes, such as Ramsey interferometry [28], coherent population control [29], and polarization modulation [30]. The technology for constructing long air waveguides has achieved experimentally successful realization of a 45-meter "fiber" in the air [31]. These all motivate thorough analysis of the roles of various mechanisms involved in the backward air lasing process in a relatively long medium, in order to envisage its efficient quantum control.

Essentially, backward lasing signals from long medium far away provide more practical information to single standoff detectors. Although the above studies have detected backward signals in short medium, it is still challenging to extend the experiment into a longer one. To explore the underlying physical mechanism, we have studied the competitive effect between forward- and backward-propagating collective spontaneous emission in a cylinder medium. We conducted thorough investigation of the conditions in the parameter space that can be beneficial to the formation of backward lasing in a long medium, since the backward lasing is a major motivation of the lasing in oxygen atoms and in air without cavity [2], but it is more difficult to propagate for long distance than the forward lasing mode.

The present paper presents the parameter conditions in need of efficient backward lasing. In the following text, we theoretically study the backward collective emission of oxygen atoms pumped by single-pass lasing, as well as its forward counterpart. Especially, we showcase that the backward superfluorescence of the oxygen atom system can be favorably realized under the condition of short gain length, low atom density and moderate collisional decoherence rate, which balance the competition between the forward and backward lasing processes.

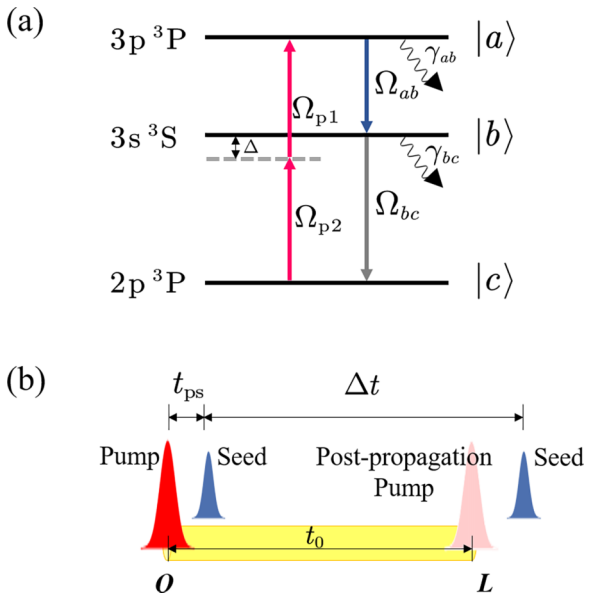

FIG. 1. Schematic of oxygen atom air laser. (a) Three-level model of oxygen atom involved in the air lasing process. Ω_{p1}, Ω_{p2}, Ω_{ab}, Ω_{bc} are the Rabi frequencies. γ_{ab} and γ_{bc} are the spontaneous emission rate of the transitions $|a\rangle \leftrightarrow |b\rangle$ and $|b\rangle \leftrightarrow |c\rangle$, respectively. (b) The air lasing scheme. A 20 ps pump pulse of 226 nm central wavelength is sent from the left end into a pencil-like medium of length L at 0.5 ns, which takes $t_0 = L/c$ to propagate through the medium and c is the group velocity. A pulse for mimicking the seed for forward lasing is injected after a delay of t_{ps}, and the seed-mimicking backward signal is injected from the right end of the medium at time $t = t_{ps} + \Delta t$. The forward (backward) signal is detected at the left (right) end of the medium.

II. THEORETICAL MODEL

Oxygen atoms generate 845 nm superfluorescence radiation in two opposite directions under the pump by the 226 nm intense laser field (see Fig. 1). This superfluorescence process belongs to the conjugated superfluorescence emission [10,14,17] from three-level cascade system [see Fig. 1(a)]. Due to the prohibition of single-photon dipole transition between the highest and lowest energy levels, the two-photon excitation is implemented to realize the population inversion between $2p\ ^3P$ (labeled as $|c\rangle$) state and $3p\ ^3P$ (labeled as $|a\rangle$) state. After that, a spontaneous relaxation process from $|a\rangle$ state to state $3s\ ^3S$ (labeled as $|b\rangle$) occurs, emitting a fluorescence pulse of 845 nm, which could form forward and backward superfluorescence in the atomic gas systems. For lacking of established population inversion between $|b\rangle$ and $|c\rangle$ state, there is only forward 130 nm UV field emitted in the $|b\rangle \leftrightarrow |c\rangle$ transition based on the phase matching condition, while the backward radiation is absent.

These processes are included in our theoretical model to analyze the backward superfluorescence. We use the Maxwell-Bloch equations (MBE) to model the dynamics of the radiation process of oxygen atoms under picosecond pulse pumping, in order to investigate the effect of medium length,

atom density, and collisional decoherence to the backward air lasing. The Hamiltonian for this three-level cascade system pump-radiation process in the interaction picture reads [17]

$$H_{\mathrm{I}} = H_{\mathrm{p}} + H_{\mathrm{g}}, \tag{1}$$

where

$$\begin{aligned} H_{\mathrm{p}} =& -\hbar\Omega_{\mathrm{p1}}\mathrm{e}^{-i\Delta t+ik_{\mathrm{p}}z}|a\rangle\langle b| - \hbar\Omega_{\mathrm{p2}}\mathrm{e}^{i\Delta t+ik_{\mathrm{p}}z}|b\rangle\langle c| + \mathrm{H.c.} \\ H_{\mathrm{g}} =& -\hbar(\Omega_{ab}^{+}\mathrm{e}^{ik_{ab}z} + \Omega_{ab}^{-}\mathrm{e}^{-ik_{ab}z})|a\rangle\langle b| \\ & -\hbar(\Omega_{bc}^{+}\mathrm{e}^{ik_{bc}z} + \Omega_{bc}^{-}\mathrm{e}^{-ik_{bc}z})|b\rangle\langle c| + \mathrm{H.c.}\,; \end{aligned} \tag{2}$$

H_{p} relates to the coherent two-photon pumping process from $|c\rangle$ state to $|a\rangle$ state, while H_{g} represents the corresponding radiation fields from the transitions $|a\rangle \leftrightarrow |b\rangle$ and $|b\rangle \leftrightarrow |c\rangle$. h.c. denotes the Hermitian conjugate. With a small detuning Δ (6.1×10^{15} rad/s) between the pump field and both the $|a\rangle \leftrightarrow |b\rangle$ and $|b\rangle \leftrightarrow |c\rangle$ transition, the two-photon excitation process is treated as two allowed transitions. The electric field of the pump pulse is expressed as $E_{\mathrm{p}} = E_0\mathrm{e}^{-i(\omega_{\mathrm{p}}t-k_{\mathrm{p}}z)} + E_0^{*}\mathrm{e}^{i(\omega_{\mathrm{p}}t-k_{\mathrm{p}}z)}$, where E_0 is the slow-varying envelope of the pump electric field, ω_{p} is the frequency of the pump pulse, and k_{p} is the wave vector, while we represents the forward and backward propagation of the field by taking positive and negative values of z. $\Omega_{\mathrm{p1}} = d_{ab}E_0/\hbar$ and $\Omega_{\mathrm{p2}} = d_{bc}E_0/\hbar$ are the Rabi frequency of pump field for the $|a\rangle \leftrightarrow |b\rangle$ and $|b\rangle \leftrightarrow |c\rangle$ transitions, while d_{ab} and d_{bc} are electric dipole matrix elements with $d_{ab} \sim 1.38 \times 10^{-29}$ C m and $d_{bc} \sim 0.38 \times 10^{-29}$ C m [17]. The radiation fields generated between the energy levels of $|a\rangle \leftrightarrow |b\rangle$ and $|b\rangle \leftrightarrow |c\rangle$ can be expressed as $\Omega_{ij}^{+}\mathrm{e}^{-i(\omega_{ij}t-k_{ij}z)} + \Omega_{ij}^{-}\mathrm{e}^{-i(\omega_{ij}t+k_{ij}z)}$, $(ij = ab, bc)$. $\Omega_{ij}^{\pm}$ are the slow-varying envelopes of the radiation fields, with positive and negative signs indicating forward and backward propagation.

In our simulation, the rotating-wave approximation, slow-varying envelope approximation and four-wave mixing approximation are applied. The temporal evolution of the density matrix ρ follows the Liouville's equation [32]

$$\frac{\partial\rho}{\partial t} = -\frac{i}{\hbar}[H_{\mathrm{I}}, \rho] + \mathcal{L}\rho. \tag{3}$$

The relaxation and decoherence effects in the oxygen air laser system are represented by $\mathcal{L}\rho$ in Eq. (3), which takes the form as

$$\begin{aligned} \mathcal{L} =& -\gamma_{ab}|a\rangle\langle a| + (\gamma_{ab} - \gamma_{bc})|b\rangle\langle b| \\ & -\left[\left(\tfrac{1}{2}(\gamma_{ab} + \gamma_{bc}) + \gamma_{\mathrm{c}}\right)|a\rangle\langle b| + \left(\tfrac{1}{2}\gamma_{bc} + \gamma_{\mathrm{c}}\right)|b\rangle\langle c|\right. \\ & \left. + \left(\tfrac{1}{2}\gamma_{ab} + \gamma_{\mathrm{c}}\right)|a\rangle\langle c| + \mathrm{H.c.}\right]. \end{aligned} \tag{4}$$

γ_{ab} and γ_{bc} are the spontaneous emission rates of the transitions $|a\rangle \leftrightarrow |b\rangle$ and $|b\rangle \leftrightarrow |c\rangle$, with $\gamma_{ab} = 9.3 \times 10^{6}$ s^{-1} and $\gamma_{bc} = 1.97 \times 10^{8}$ s^{-1}, while γ_{c} is the collisional decoherence rate [17] which can be manipulated. The evolution of the generated fields $\Omega_{ab}^{\pm}$ and $\Omega_{bc}^{\pm}$ follows the Maxwell equation

$$\frac{1}{c}\partial_t\Omega_{ab}^{\pm} \pm \partial_z\Omega_{ab}^{\pm} + \kappa\Omega_{ab}^{\pm} = i\eta_{ab}\rho_{ab}^{\pm}, \tag{5}$$

$$\frac{1}{c}\partial_t\Omega_{bc}^{\pm} \pm \partial_z\Omega_{bc}^{\pm} = i\eta_{bc}\rho_{bc}^{\pm}. \tag{6}$$

In Eqs. (5) and (6), $\eta_{ij} = \frac{3}{8\pi}n\lambda_{ij}^{2}\gamma_{ij}$ is the coupling constant between atoms and field, where n is the excited atomic density and λ_{ij} is the wavelength of the corresponding field. $\kappa \sim 1.5$ cm^{-1} is depletion rate of the 845 nm field due to the Rayleigh diffraction length [17,33].

We inject a 226 nm Gaussian laser pulse, at 0.5 ns and the peak power of 7.65×10^{9} W/cm^2, entering a pencil-like mirrorless active volume of $L = 1$ cm medium length, which is similar to those used in the experiment [14], into the left boundary of the medium to activate the oxygen. In our simulation, we find that as long as enough population inversion from state $|a\rangle$ to state $|c\rangle$ is generated by the 226 nm pump pulse, there is little difference between a long nanosecond pump pulse and a shorter picosecond one. So we use a pump pulse of 20 ps full width at half maximum (FWHM) in the simulation. The cross-section radius of the cylindrical medium is rather small ($r \ll L$). After $t_{\mathrm{ps}} = 0.01$ ns interval time, we send a forward Gaussian seed pulse (of 10^5 rad/s peak Rabi frequency) at the same position. The backward seed is injected from the right end of the active medium at $t = t_{\mathrm{ps}} + \Delta t$. Δt is the time delay between forward and backward seed. We assume the seed pulses generated at both ends of the medium are sufficiently amplified after propagation. As our simulation shows that the Rabi frequency of the Gaussian seed pulse neither changes the magnitude of the emitting pulse or the underlying physics, it may be acceptable to consider the seed pulse as a spontaneous emission source in the large gain regime [34]. The detailed simulation about the Rabi frequency of the seed pulse is shown in Appendix B. For the standoff detection [2], the backward seed carrying farthest information generates at the time when the pump pulse has propagated out of the interaction zone, namely, it lags behind the forward seed by the time t_0.

In order to get the farthest medium information, we set the medium length to be $L = 5$ cm compared with the $L = 1$ cm simulation, changing the atom density and the collisional decoherence rate, to observe the optimal condition for remote sensing.

III. RESULTS AND DISCUSSION

We demonstrate that in the bidirectional coherent radiation of oxygen atoms, the length of the gain medium L, the atom density n, and the collisional decoherence rate γ_{c} have important effects on the optical amplification. Our simulation for the collisional decoherence rate is on a scale from 0.1 ns^{-1} to 500 ns^{-1} which contains the 1×10^{10} s^{-1} in the actual experiment. As the collisional decoherence rate is actually effected by the density of the gas, the temperature of the environment which affects the incoming collisional velocity, as well as the scattering cross section and so on, it is achievable to adjust it in some ways, such as lowering the temperature [35,36]. Firstly we show the spatial-temporal evolution of the generated 845 nm forward and backward fields inside the $L = 1$ cm gain medium in Figs. 2(a) and 2(b), with $\gamma_{\mathrm{c}} = 10$ ns^{-1} and $n = 1 \times 10^{21}$ m^{-3} as in the experiment. It can be identified that the forward field Ω_{ab}^{+} acts as superfluorescence with high intensity ($\sim 10^{11}$ rad/s), short time delay ($\sim$0.022 ns), and ringing effect in the latter half of the medium. The larger the gain length is, the stronger intensity Ω_{ab}^{+} is built up to. Similarly, the backward field Ω_{ab}^{-} is also amplified in the form of superfluorescence to the same order ($\sim 10^{11}$ rad/s) of its

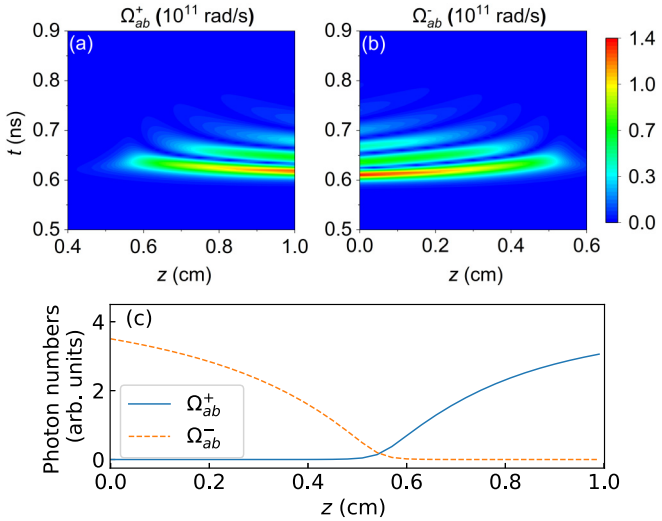

FIG. 2. Air lasing in the short ($L = 1$ cm) gain medium of oxygen atoms. Spatial and temporal evolution of the generated 845 nm (a) forward (b) backward field intensities, and (c) time-integrated photon numbers.

Rabi frequency as the forward one, while in contrast at the forepart of the gain region.

The energy gain, presented as time-integrated photon numbers, increases linearly at first, which is a typical character of superfluorescence, and then turns to saturation with the changing propagating extent as indicated in Fig. 2(c). In this scenario, the collective radiations emit under the formation of macroscopic dipole moment and both the forward- and backward-propagating signals are amplified, resulting in a competitive behavior for the population inversion. Theoretically, the amplified fields contain information from the entire medium. It is noteworthy that the forward signal carries more information about the latter part of the medium, whereas the backward one conveys information predominantly related to the front segment. The significant amplified backward signal obtained in this 1 cm active medium can be used to detect the atomic distribution information mainly at half of the total length within this range.

As the gain length is extend to $L = 5$ cm, the forward and backward fields generated at 845 nm exhibit distinct behaviors.

For the pump pulse with 20 ps FWHM, we assume that the medium length from several millimeters to 1 cm is in the short medium regime, while medium length $L > 1$ cm is considered to be a long medium. Figure 3 illustrates the population dynamics in a medium of length $L = 5$ cm, along with the simulated temporal evolutions of the forward and backward 845 nm fields. The simulation is conducted with a constant atomic oxygen density of $n = 1 \times 10^{21}$ m^{-3} and a collisional decoherence rate of $\gamma_c = 10$ ns^{-1}. The 845 nm field intensity is represented by its corresponding Rabi frequency $\Omega^{\pm}_{ab}$. As shown in Fig. 3(a), the forward field Ω^+_{ab} is amplified to a Rabi frequency of 3×10^{11} rad/s, which falls within the superfluorescence region with a short time delay and rapid oscillation (ringing effect). In contrast, the backward field Ω^-_{ab} undergoes minimal amplification [see Fig. 3(c)],

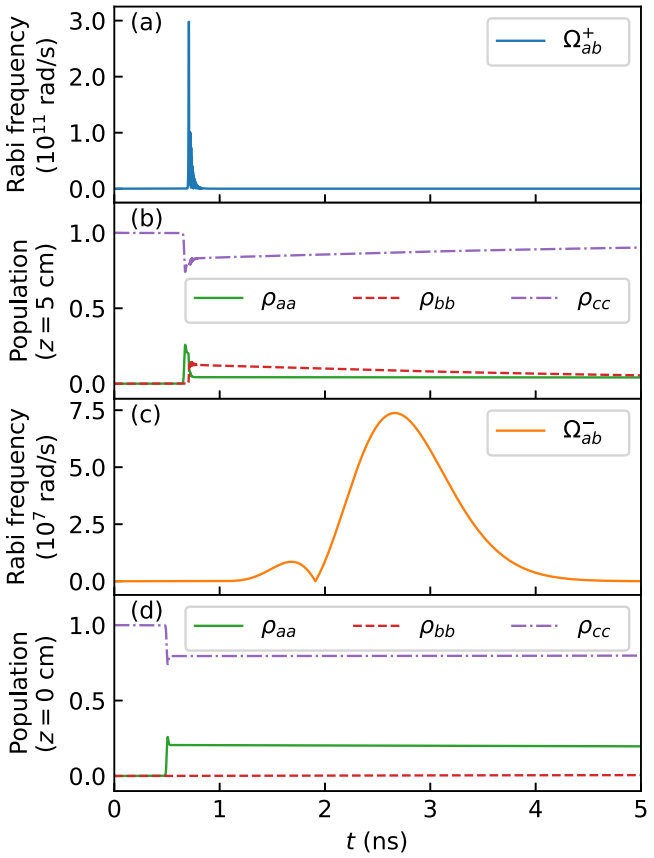

FIG. 3. (a) and (c): Temporal behaviors of the generated 845 nm forward (Ω^+_{ab}) and backward (Ω^-_{ab}) emission in the $L = 5$ cm medium with other parameters the same as Fig. 2. (b) and (d): The population dynamics of oxygen atoms at the right ($z = 5$ cm) and left ($z = 0$ cm) end of the medium which are corresponding to Ω^+_{ab} and Ω^-_{ab}.

with a maximum Rabi frequency of 7.5×10^7 rad/s, which is four orders of magnitude lower than that of the forward field.

The underlying reason for the suppression of backward lasing in the extended medium is the competition for population inversion between the lasing processes propagating in both directions. Figures 3(b) and 3(d) depict the corresponding population dynamics of $\Omega^{\pm}_{ab}$. The population of the system is transferred from the initial ground state $|c\rangle$ to the excited state $|a\rangle$ under the pump of the UV pulse, creating population inversion between the $|a\rangle$ and $|b\rangle$ states. For the superfluorescence emission process, the macroscopic dipole moment is gradually built up through spontaneous radiation and dipole-dipole interaction. Following a certain time delay, a strong superfluorescent radiation is emitted due to the $|a\rangle \leftrightarrow |b\rangle$ transition, while the population is transferred from $|a\rangle$ to $|b\rangle$ state, leading to a reduction in the degree of population inversion. Due to the time delay between the forward and backward seeds caused by the propagation of the pump field, Ω^+_{ab} is easily amplified, consuming most of the population inversion, while Ω^-_{ab} is suppressed.

To be more specific, the dominant parameters, principally atom density and dephasing rate which determine the coherent superfluorescence radiation process in an extended medium, are investigated. The peak Rabi frequencies under various atomic density and collisional decoherence are studied in

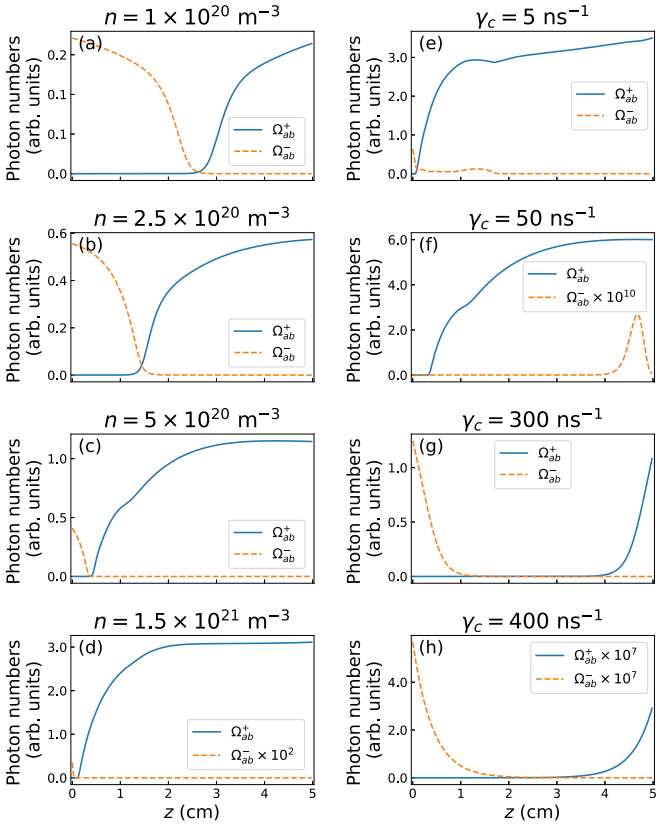

FIG. 4. Time-integrated photon numbers for the forward- and backward-propagating lasing signals in a $L = 5$ cm gain medium at selected atom densities n: (a) $n = 1 \times 10^{20}$ m^{-3}, (b) $n = 2.5 \times 10^{20}$ m^{-3}, (c) $n = 5 \times 10^{20}$ m^{-3}, (d) $n = 1.5 \times 10^{21}$ m^{-3}, and dephasing rates γ_c: (e) $\gamma_c = 5$ ns^{-1}, (f) $\gamma_c = 50$ ns^{-1}, (g) $\gamma_c = 300$ ns^{-1}, (h) $\gamma_c = 400$ ns^{-1}.

Appendix C. In Fig. 4, we present the time-integrated photon numbers at selected parameters, for the forward and backward propagating lasing signals with respect to the medium spatial coordinate axis. Regarding atom density, the backward signals exhibit a decreasing trend as n increases. In Fig. 4(a), for a small atom density of $n = 1 \times 10^{20}$ m^{-3}, both forward and backward emissions are amplified, starting from the middle of the 5 cm medium. However, as the density increases in Figs. 4(b)–4(d), the amplification starting positions gradually shift towards the left side of the medium ($z = 0$), resulting in a continuous decrease of backward signals, while the forward photon numbers keep accumulating.

When it comes to dephasing rate as indicated in Figs. 4(e)–4(h), the amplifications get more intricate. At small dephasing rates $\gamma_c = 5$ ns^{-1} and [see Figs. 4(e), 4(f)], the amplification processes are dominated by forward emissions, resulting in weak backward fields. However, counterintuitively, when $\gamma_c = 300$ ns^{-1} in Fig. 4(g), both the forward and backward emissions are amplified, although both fields carry little information about the middle of the medium. The reason for this long-gain medium's backward amplification is that the forward field is either greatly weakened due to a large decoherence rate, or it is suppressed due to the absence of population inversion. In the limit of a large decoherence rate [$\gamma_c = 400$ ns^{-1}, Fig. 4(h)], both fields are suppressed, because the polarization is not easily built up under this large decoherence rate.

Through the above analysis, we show that the forward radiation will be amplified continuously with the increase of atom density at large medium length, and a strong collective spontaneous radiation process will occur, while the backward amplification is more inclined to occur under the short medium length, or only in a certain low-atom density interval when the medium is long. In the population-inverted system, the coherence effects play the dominant role in a wide range of decoherence rates, resulting in SF radiation mainly in the forward direction, while in the large or quite small decoherence rate limit, backward amplification appears to a certain extent.

Our simulations point out the major mechanism of suppressing the backward lasing process to be the competition of forward lasing, which exhausts the population of the $|a\rangle$ state when the backward-propagating seed is still to be amplified. Especially for the case of air lasing in the long medium, the forward radiation field could be too strong after propagating through long gain length and weakens the degree of population inversion in the medium, which overwhelms the amplification of the backward seeding field close to the right end of the medium. Due to this mechanism, lower atom density and moderate decoherence rate can counterintuitively enhance the backward amplification process, since these conditions can balance the amplification dynamics of forward and backward propagating fields, thus leaving space and time for the backward seeding field to be sufficiently amplified. On the other hand, certain mechanisms such as variation of backward seeding delay could possibly alleviate the suppression of backward amplification.

The temporal asymmetry of the forward and backward fields is generated because of the temporal asymmetry of the forward and backward seed pulses due to the propagation effect of the pump pulse, which leads to the competition between amplifications of the forward and backward fields.

We have gotten the conclusion that both the forward and backward propagating fields will be amplified inside an $L = 1$ cm oxygen atom gain medium at specific parameters. From the perspective of propagating time, since it takes 30 ps for the pump pulse to pass through the 1 cm medium, the medium undergoes a uniform population inversion when being pumped by the 20 ps lasing pulse, so the temporal asymmetry for the forward and backward seeds caused by time delay is small, which leads to almost equal amplified bidirectional superfluorescent radiation (see Appendix A). When the medium length is larger ($L = 5$ cm), the pump pulse needs 167 ps to pass through the medium. In this case, the time delay between two seeds is large, which leads to an obvious temporal asymmetry, so that the forward field is amplified along the cylinder, while the backward field is difficult to be amplified.

We propose an alternative approach to enhance the 845 nm backward lasing signal, by reducing the time delay Δt between the two seeds, as shown in Fig. 5. For the $L = 5$ cm medium without time delay of seeds ($\Delta t = 0$ ps), the forward and backward field are all sufficiently amplified to high Rabi frequencies with narrow pulse widths and ringing effects as shown in Figs. 5(a) and 5(e). When the time delay

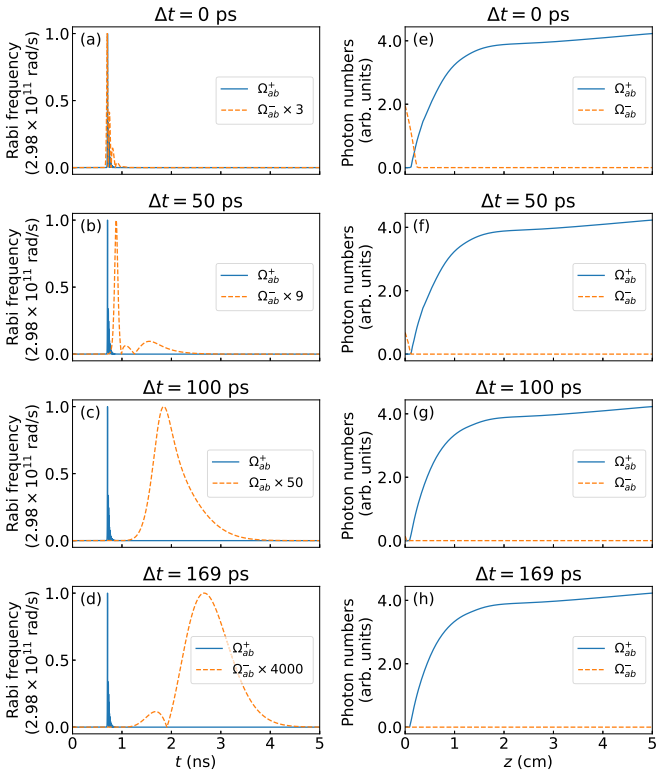

FIG. 5. Temporal behaviors (left panel) and time-integrated photon numbers (right panel) of the generated 845 nm forward and backward fields in a $L = 5$ cm medium with different initial time delay Δt between the forward seed and backward seed: (a) and (e) $\Delta t = 0$ ps, (b) and (f) $\Delta t = 50$ ps, (c) and (g) $\Delta t = 100$ ps, (d) and (h) $\Delta t = 167$ ps which equals to the time the pump pulse takes to travel through the whole $L = 5$ cm medium.

is introduced, the forward fields prevail in the competition and maintain the $\sim 3 \times 10^{11}$ rad/s peak Rabi frequencies in Figs. 5(b)–5(d), while the backward fields are gradually suppressed so that they turn from the strong-oscillating SF to weak-oscillating SF [Fig. 5(f)], and to amplified spontaneous emission (ASE) [Figs. 5(g) and 5(h)]. So as long as we can control the pump process, for example a homogeneous pumping, or the seed generating time, we will get the amplified backward lasing.

IV. CONCLUSION

To summarize, the forward and backward 845 nm superfluorescences of oxygen atoms are discussed in a simplified three-level UV single-pass pump model. We studied the long medium amplification, and mainly focused on the physical mechanism and parameter conditions of the backward lasing. For a long population-inverted medium, lower atom density will help for the formation of backward emission. In terms of the collisional decoherence, we find that in a wide range of decoherence rate, only the forward field is amplified for a long medium, while in the large or small decoherence rate limit, the backward emission can be amplified to some extent. Backward lasing will be accomplished at small forward and backward seeds' time delay. This work provides theoretical guidance for the implementation of backward air laser, and insight of roles of various physical mechanisms in the forward and backward emission.

ACKNOWLEDGMENTS

Grants from NSFC (Grants No. 12374238, No. 11934004, No. 11974230, No. 12174009, No. 12234002, No. 92250303, and No. 12304279) and Beijing Natural Science Foundation (Grant No. Z220008) are gratefully acknowledged. Y.H.K. and W.T.L. are supported by the National Science and Technology Council of Taiwan, ROC (Grants No. 110-2112-M-008-027-MY3, and No. 111-2923-M-008-004-MY3). W.T.L. acknowledges support from Center for Quantum Technology, Hsinchu 30013, Taiwan, ROC.

APPENDIX A: UNIFORM PUMP

In Fig. 6 we show the simulated results for an $L = 5$ cm long uniformly pumped medium. The Rabi frequency of the pump pulse is the same as the mentioned peak Rabi frequency of the Gaussian pulse in Section II. As we can see, both the forward and backward fields are amplified to the order of 10^{11} rad/s. The complex structures are the results from the uniform pump pulse which lead to stronger atom-field interactions.

APPENDIX B: PEAK INTENSITY OF SEED PULSE

In Fig. 7, we show the effect of the seed Rabi frequency (Ω_s) on the generated 845 nm backward field in an $L = 1$ cm medium with other parameter conditions the same as Fig. 2. The results show that the Rabi frequency of the Gaussian seed pulse does not change the magnitude of the emitting pulse (10^{11} rad/s) as well as the underlying physics, even though it has slight influence on the emission time delay and the intensity. According to Fig. 7, even for a seed pulse with $\Omega_s = 10$

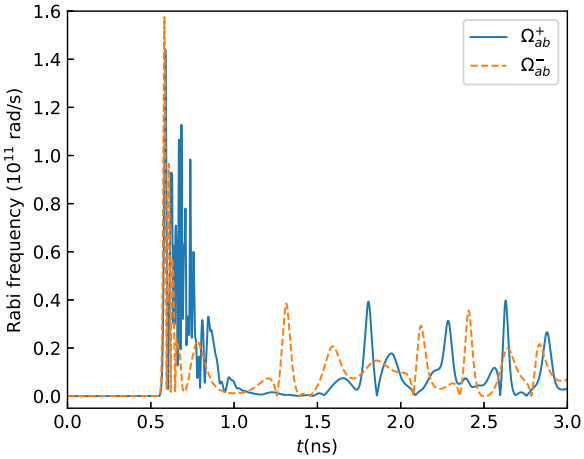

FIG. 6. Temporal behavior of the generated 845 nm forward (Ω^+_{ab}) and backward (Ω^-_{ab}) fields in an $L = 5$ cm medium which is uniformly pumped.

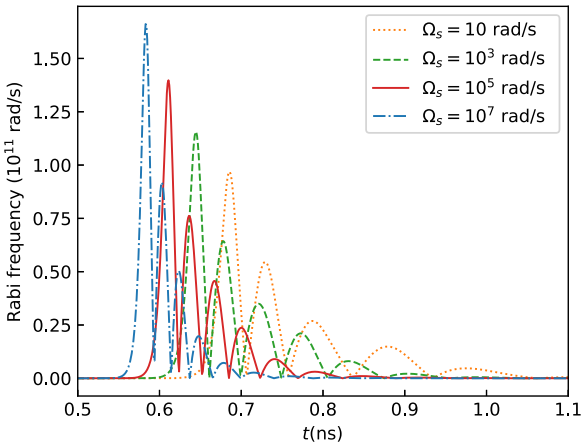

FIG. 7. Temporal behavior of the generated 845 nm backward fields (Ω_{ab}^{-}) in an $L = 1$ cm medium for different incident Gaussian seed peak intensities.

rad/s there is still a strong coherent superfluorescence emitted. So we believe that this simulation with a seeded pulse is also a good mimic to the spontaneous radiation process.

APPENDIX C: PEAK RABI FREQUENCY FOR VARIOUS ATOMIC DENSITY AND COLLISIONAL DECOHERENCE RATE

In terms of atom density, we obtained the peak Rabi frequency of the coherent emission for the atom density from 1×10^{19} m^{-3} to 2×10^{21} m^{-3} and medium length from 1 cm to 10 cm in Fig. 8. The simulation results show that with the increase of atom density, the peak Rabi frequency of forward emission for all L gradually increases. However, for the 845 nm backward field, only short medium could generate the superfluorescence in broad atom density, while for the long L the signals are produced only in the regime of low atom density. We also present the investigation of the effect of dephasing via collisional decoherence, which is phenomenologically included in the model for the forward and backward coherent emission through the collisional decoherence rate γ_c. The peak Rabi frequency of the forward and backward collective emission at decoherence rate from 0.1 ns^{-1} to 500 ns^{-1} and gain length from 1 cm to 10 cm are shown in Fig. 9.

For the forward emission Ω_{ab}^{+}, the collisional decoherence rate γ_c has the same influence for all L, namely, with its

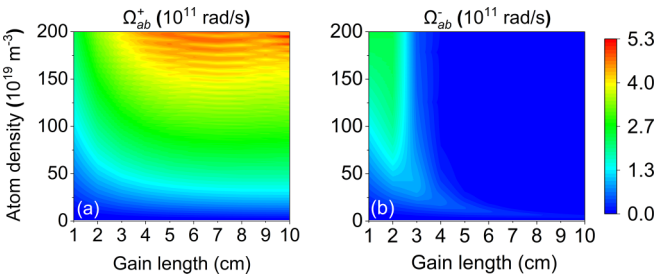

FIG. 8. Peak Rabi frequency of generated 845 nm (a) forward and (b) backward fields depending on the atom density and medium length.

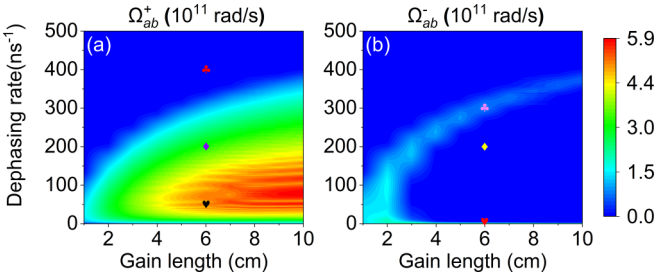

FIG. 9. Peak Rabi frequency of generated 845 nm (a) forward and (b) backward fields depending on the collisional decoherence rate and medium length.

increase, the peak Rabi frequency of the forward field always gets stronger first and then decreases, as shown in Fig. 9(a). The reason for the increase region of Ω_{ab}^{+} with the rise of γ_c is because smaller decoherence rate has a certain effect on the formation of macroscopic polarization of the oxygen cascade system. Thus, with the increase of γ_c, the intensity of radiation field gradually increases. On the contrary, when γ_c gets larger, it leads to the collisional decoherence that is much faster than the evolution of the polarization, so that the coherent effects lose the dominant influence and the emission field turns to fluorescence.

As to the backward propagating field, Ω_{ab}^{-} has two amplified spontaneous emission regions under the influences of γ_c and L as shown in Fig. 9(b): when γ_c is rather small, there is strong backward propagating SF emitting at all L; with larger γ_c distributing at different L, weak SF happens. Besides these two amplification parameter conditions, the coherent radiation signals are quite weak. So the collisional decoherence effect and the gain length have a stronger impact on the backward SF compared to the forward amplification.

For small L, the forward and backward fields will be amplified simultaneously as revealed in Fig. 9. The reason for the backward amplification at long gain length is that the forward field is either greatly weakened due to large decoherence rate, or it is suppressed due to absence of population inversion. Then we show the temporal profiles of the 845 nm forward and backward fields at $L = 6$ cm with several decoherence rates, which correspond to the six tagged points in Fig. 9. Figures 10(a)–10(c) represent the three points from top to bottom in Fig. 9(a), and Figs. 10(d)–10(f) represent the points for top to bottom in Fig. 9(b).

In the large decoherence rate limit in Fig. 10(a), the forward emission Ω_{ab}^{+} turns to ASE with a broad pulse width and low peak Rabi frequency of 9×10^7 rad/s, for the reason that the polarization is not easy to be built up under large decoherence rate. With γ_c getting smaller, the collective coherence effect gradually grows and becomes dominant, which leads to the normal SF in Fig. 10(b) with 3×10^{11} rad/s peak Rabi frequency and the stronger SF with narrower pulse width of 5×10^{11} rad/s Rabi frequency in Fig. 10(c). The backward field Ω_{ab}^{-} is amplified in Figs. 10(d) and (f), respectively, to the damped SF with 8×10^{10} rad/s peak Rabi frequency and the strong-oscillatory SF with 3×10^{11} rad/s peak Rabi frequency, while at other decoherence rate intervals, such as Fig. 10(e), Ω_{ab}^{-} can be attributed to weak ASE with ca. 3×10^6 rad/s peak Rabi frequency.

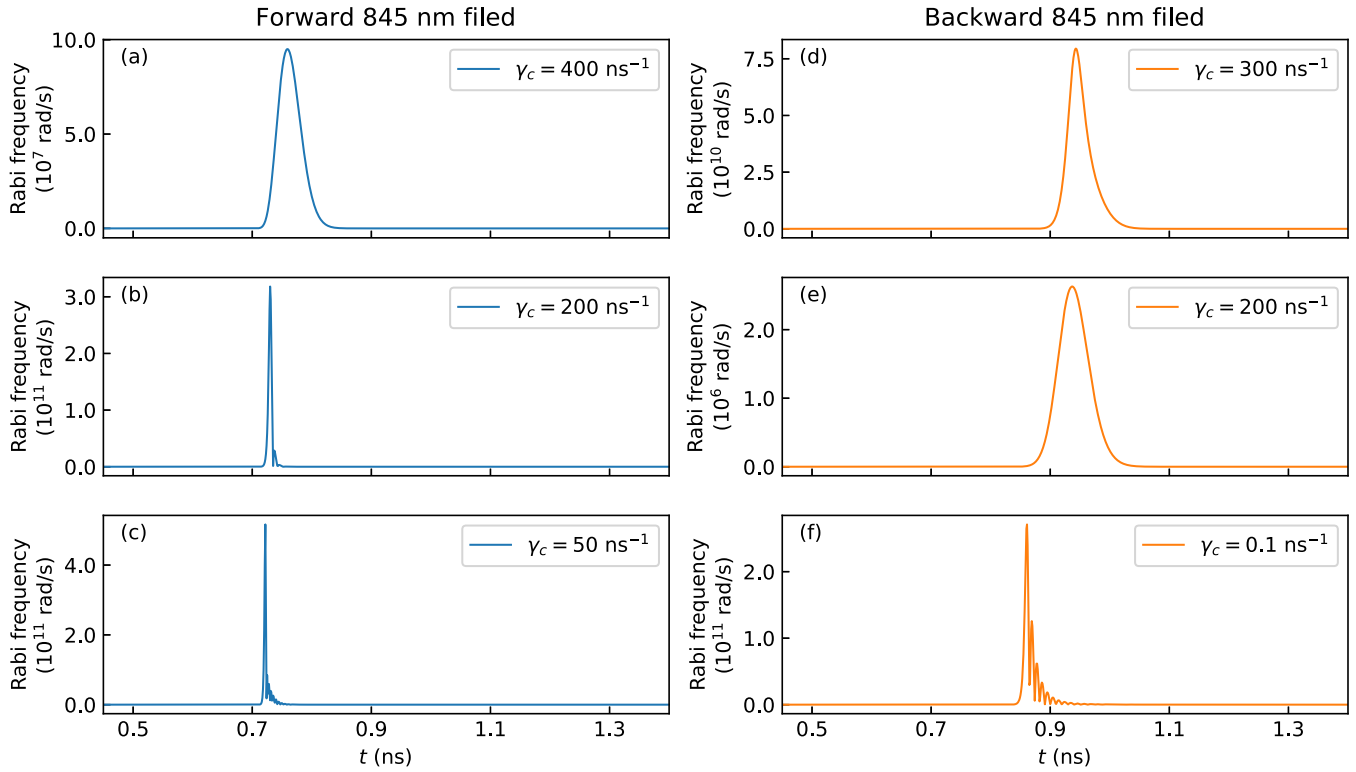

FIG. 10. Temporal behavior of the generated 845 nm forward (Ω_{ab}^{+}) and backward (Ω_{ab}^{-}) fields in a $L = 6$ cm medium with different collisional decoherence rates where the simulating parameters are corresponding to the tags in Fig. 9: (a) Ω_{ab}^{+} with $\gamma_c = 400$ ns^{-1} [Fig. 9(a) red club], (b) Ω_{ab}^{+} with $\gamma_c = 200$ ns^{-1} [Fig. 9(a) purple diamond], (c) Ω_{ab}^{+} with $\gamma_c = 50$ ns^{-1} [Fig. 9(a) black heart], (d) Ω_{ab}^{-} with $\gamma_c = 300$ ns^{-1} [Fig. 9(b) pink club], (e) Ω_{ab}^{-} with $\gamma_c = 200$ ns^{-1} [Fig. 9(b) white diamond], (f) Ω_{ab}^{-} with $\gamma_c = 0.1$ ns^{-1} [Fig. 9(b) red heart].

[1] Q. Luo, W. Liu, and S. L. Chin, Lasing action in air induced by ultra-fast laser filamentation, Appl. Phys. B: Lasers Opt. **76**, 337 (2003).

[2] A. Dogariu, J. B. Michael, M. O. Scully, and R. B. Miles, High-gain backward lasing in air, Science **331**, 442 (2011).

[3] J. Yao, B. Zeng, H. Xu, G. Li, W. Chu, J. Ni, H. Zhang, S. L. Chin, Y. Cheng, and Z. Xu, High-brightness switchable multiwavelength remote laser in air, Phys. Rev. A **84**, 051802(R) (2011).

[4] P. R. Hemmer, R. B. Miles, P. Polynkin, T. Siebert, A. V. Sokolov, P. Sprangle, and M. O. Scully, Standoff spectroscopy via remote generation of a backward-propagating laser beam, Proc. Natl. Acad. Sci. USA **108**, 3130 (2011).

[5] L. Yuan, K. E. Dorfman, A. M. Zheltikov, and M. O. Scully, Plasma-assisted coherent backscattering for standoff spectroscopy, Opt. Lett. **37**, 987 (2012).

[6] M. Ruchkina, P. Ding, A. Ehn, M. Aldén, and J. Bood, Single-shot, spatially-resolved stand-off detection of atomic hydrogen via backward lasing in flames, Proc. Combust. Inst. **37**, 1281 (2019).

[7] L. Yuan and A. A. Svidzinsky, Gain without population inversion in a yoked superfluorescence scheme, Phys. Rev. A **85**, 033836 (2012).

[8] R. H. Dicke, Coherence in spontaneous radiation processes, Phys. Rev. **93**, 99 (1954).

[9] R. Bonifacio and L. A. Lugiato, Cooperative radiation processes in two-level systems: Superfluorescence, Phys. Rev. A **11**, 1507 (1975).

[10] J. H. Brownell, X. Lu, and S. R. Hartmann, Yoked superfluorescence, Phys. Rev. Lett. **75**, 3265 (1995).

[11] D. Polder, M. F. H. Schuurmans, and Q. H. F. Vrehen, Superfluorescence: Quantum-mechanical derivation of Maxwell-Bloch description with fluctuating field source, Phys. Rev. A **19**, 1192 (1979).

[12] F. Haake, H. King, G. Schröder, J. Haus, and R. Glauber, Fluctuations in superfluorescence, Phys. Rev. A **20**, 2047 (1979).

[13] A. I. Lvovsky, S. R. Hartmann, and F. Moshary, Omnidirectional superfluorescence, Phys. Rev. Lett. **82**, 4420 (1999).

[14] A. J. Traverso, R. Sanchez-Gonzalez, L. Yuan, K. Wang, D. V. Voronine, A. M. Zheltikov, Y. Rostovtsev, V. A. Sautenkov, A. V. Sokolov, S. W. North, and M. O. Scully, Coherence brightened laser source for atmospheric remote sensing, Proc. Natl. Acad. Sci. USA **109**, 15185 (2012).

[15] A. Laurain, M. Scheller, and P. Polynkin, Low-threshold bidirectional air lasing, Phys. Rev. Lett. **113**, 253901 (2014).

[16] Y. V. Rostovtsev, Z. E. Sariyanni, and M. O. Scully, Electromagnetically induced coherent backscattering, Phys. Rev. Lett. **97**, 113001 (2006).

[17] L. Yuan, B. H. Hokr, A. J. Traverso, D. V. Voronine, Y. Rostovtsev, A. V. Sokolov, and M. O. Scully, Theoretical

analysis of the coherence-brightened laser in air, Phys. Rev. A **87**, 023826 (2013).

[18] E. L. Bolda, R. Y. Chiao, and J. C. Garrison, Superfluorescence in a continuously pumped medium, Phys. Rev. A **52**, 3308 (1995).

[19] P. W. Hoff, H. A. Haus, and T. J. Bridges, Observation of optical nutation in an active medium, Phys. Rev. Lett. **25**, 82 (1970).

[20] G. Panitchayangkoon, D. Hayes, K. A. Fransted, J. R. Caram, E. Harel, J. Wen, R. E. Blankenship, and G. S. Engel, Long-lived quantum coherence in photosynthetic complexes at physiological temperature, Proc. Natl. Acad. Sci. USA **107**, 12766 (2010).

[21] P. Ding, C. Brackmann, M. Ruchkina, M. Zhuzou, L. Wang, L. Yuan, Y. Liu, B. Hu, and J. Bood, Femtosecond laser-induced quantum-beat superfluorescence of atomic oxygen in a flame, Phys. Rev. A **104**, 033517 (2021).

[22] L. Yuan, A. A. Lanin, P. K. Jha, A. J. Traverso, D. V. Voronine, K. E. Dorfman, A. B. Fedotov, G. R. Welch, A. V. Sokolov, A. M. Zheltikov, and M. O. Scully, Coherent Raman umklapp-scattering, Laser Phys. Lett. **8**, 736 (2011).

[23] X. Zhang, R. Danylo, Z. Fan, P. Ding, C. Kou, Q. Liang, A. Houard, V. Tikhonchuk, A. Mysyrowicz, and Y. Liu, Backward lasing of singly ionized nitrogen ions pumped by femtosecond laser pulses, Appl. Phys. B **126**, 53 (2020).

[24] H. Lei, G. Li, H. Xie, Q. Zhang, X. Wang, J. Zhao, Z. Chen, and Z. Zhao, Mechanism and control of rotational coherence in femtosecond laser-driven N_2, Opt. Express **28**, 22829 (2020).

[25] X. Zhang, Q. Lu, Z. Zhang, Z. Fan, D. Zhou, Q. Liang, L. Yuan, S. Zhuang, K. Dorfman, and Y. Liu, Coherent control of the multiple wavelength lasing of N_2^+: coherence transfer and beyond, Optica **8**, 668 (2021).

[26] S. F. Jacobs, M. O. Scully, M. Sargent, and C. D. Cantrell, *Laser Induced Fusion and X-Ray Laser Studies: Based on Lectures of the June 23-July 4, 1975 Summer School, Sante Fe, New Mexico* (Addison-Wesley, 1975).

[27] P. Ding, M. Ruchkina, D. D. Cont-Bernard, A. Ehn, D. A. Lacoste, and J. Bood, Detection of atomic oxygen in a plasma-assisted flame via a backward lasing technique, Opt. Lett. **44**, 5477 (2019).

[28] Z. Li, Y.-H. Kuan, X. Mu, Z. Miao, C. Wu, and W.-T. Liao, Ramsey interferometry through coherent $A^2\Pi_u - X^2\Sigma_g^+ - B^2\Sigma_u^+$ coupling and population transfer in N_2^+ air laser, Opt. Lett. **45**, 6587 (2020).

[29] H. Li, E. Lotstedt, H. Li, Y. Zhou, N. Dong, L. Deng, P. Lu, T. Ando, A. Iwasaki, Y. Fu, S. Wang, J. Wu, K. Yamanouchi, and H. Xu, Giant enhancement of air lasing by complete population inversion in N_2^+, Phys. Rev. Lett. **125**, 053201 (2020).

[30] H. Li, M. Hou, H. Zang, Y. Fu, E. Lotstedt, T. Ando, A. Iwasaki, K. Yamanouchi, and H. Xu, Significant enhancement of N_2^+ lasing by polarization-modulated ultrashort laser pulses, Phys. Rev. Lett. **122**, 013202 (2019).

[31] A. Goffin, I. Larkin, A. Tartaro, A. Schweinsberg, A. Valenzuela, E. W. Rosenthal, and H. M. Milchberg, Optical guiding in 50-meter-scale air waveguides, Phys. Rev. X **13**, 011006 (2023).

[32] M. O. Scully and M. S. Zubairy, *Quantum Optics* (Cambridge University Press, 1997).

[33] R. B. Miles, W. R. Lempert, and J. N. Forkey, Laser rayleigh scattering, Meas. Sci. Technol. **12**, R33 (2001).

[34] M. S. Malcuit, J. J. Maki, D. J. Simkin, and R. W. Boyd, Transition from superfluorescence to amplified spontaneous emission, Phys. Rev. Lett. **59**, 1189 (1987).

[35] B. Vacchini, Quantum and classical features in the explanation of collisional decoherence, J. Mod. Opt. **51**, 1025 (2004).

[36] M. Schlosshauer, Quantum decoherence, Phys. Rep. **831**, 1 (2019).